

## Structural and Functional Studies of Bacterial Enolase, a Potential Target Against Gram-Negative Pathogens.

Jolanta Krucinska, Eric Falcone, Heidi Erlandsen, Akram Hazeen, Michael Nicolo Lombardo, Alexavier Estrada, Victoria Lee Robinson, Amy Anderson, and Dennis L. Wright

*Biochemistry*, **Just Accepted Manuscript** • DOI: 10.1021/acs.biochem.8b01298 • Publication Date (Web): 04 Feb 2019

Downloaded from <http://pubs.acs.org> on February 4, 2019

### Just Accepted

“Just Accepted” manuscripts have been peer-reviewed and accepted for publication. They are posted online prior to technical editing, formatting for publication and author proofing. The American Chemical Society provides “Just Accepted” as a service to the research community to expedite the dissemination of scientific material as soon as possible after acceptance. “Just Accepted” manuscripts appear in full in PDF format accompanied by an HTML abstract. “Just Accepted” manuscripts have been fully peer reviewed, but should not be considered the official version of record. They are citable by the Digital Object Identifier (DOI®). “Just Accepted” is an optional service offered to authors. Therefore, the “Just Accepted” Web site may not include all articles that will be published in the journal. After a manuscript is technically edited and formatted, it will be removed from the “Just Accepted” Web site and published as an ASAP article. Note that technical editing may introduce minor changes to the manuscript text and/or graphics which could affect content, and all legal disclaimers and ethical guidelines that apply to the journal pertain. ACS cannot be held responsible for errors or consequences arising from the use of information contained in these “Just Accepted” manuscripts.



# Structural and Functional Studies of Bacterial Enolase, a Potential Target Against Gram-Negative Pathogens.

Jolanta Krucinska<sup>1‡</sup>, Eric Falcone<sup>1‡</sup>, Heidi Erlandsen<sup>2</sup>, Akram Hazeen<sup>3</sup>, Michael N. Lombardo<sup>1</sup>, Alexavier Estrada<sup>1</sup>, Victoria Robinson<sup>2</sup>, Amy C. Anderson<sup>1</sup> and Dennis L. Wright<sup>1,3\*</sup>

<sup>1</sup>Department of Pharmaceutical Sciences, University of Connecticut, 69 N. Eagleville Rd., Storrs, CT 06269

<sup>2</sup>Center for Open Research Resources & Equipment (COR<sup>2</sup>E), 91 N. Eagleville Rd., Storrs, CT 06269

<sup>2</sup>Department of Molecular and Cellular Biology, 91 N. Eagleville Rd., Storrs, CT 06269

<sup>3</sup>Department of Chemistry, University of Connecticut, 55 N. Eagleville Rd., Storrs, CT 06269

‡These authors contributed equally to this work

\*Corresponding author

**KEYWORDS:** *Escherichia coli*, enolase, tropolone, DARTS, Gram-negative, antibiotic.

**ABSTRACT:** Enolase is a glycolytic metalloenzyme involved in carbon metabolism. The advantage of targeting enolase lies in its essentiality in many biological processes such as cell wall formation, RNA turnover and as a plasminogen receptor. We initially used a DARTS assay to identify enolase as a target in *Escherichia coli*. The antibacterial activity of  $\alpha$ -,  $\beta$ -, and  $\gamma$ -substituted seven-member ring tropolones were first evaluated against four strains representing a range of Gram-negative bacteria. We observed that the chemical properties and position of the substituents on the tropolone ring plays an important role in the biological activity of the investigated compounds. Both  $\alpha$ - and  $\beta$ - substituted phenyl derivatives of tropolone were the most active with MIC values in the range of 11-14  $\mu\text{g/mL}$ . The potential inhibitory activity of the synthetic tropolones was further evaluated using an enolase inhibition assay, X-ray crystallography and molecular docking simulations. The catalytic activity of enolase was effectively inhibited by both the naturally occurring  $\beta$ -thujaplicin and  $\alpha$ - and  $\beta$ -substituted phenyl derivatives of tropolones with  $\text{IC}_{50}$  values in range of 8 to 11  $\mu\text{M}$ . Ligand binding parameters were assessed by ITC and DSC techniques and agreed with the *in vitro* data. Our studies validate the antibacterial potential of tropolones with careful consideration of position and character of chelating moieties for stronger interaction with metal ions and residues in the enolase active site.

## INTRODUCTION

The emergence of highly drug-resistant pathogenic bacteria, especially Gram-negative organisms, highlights the critical need for development of new effective agents to compliment the current slate of clinically approved drugs.<sup>1</sup> Despite advances in high-throughput screening and knowledge-based design, natural products still represent a vital source of novel lead material. Unfortunately, even the well of natural products have yielded few new chemotypes with activity against the more challenging Gram-negative organisms.<sup>2</sup> The limited activity of many naturally occurring antibiotics against Gram-negative bacteria may relate to unfavorable physicochemical properties, such as high molecular weight and elevated logP values, that are believed to limit bacterial penetration.<sup>3</sup>

Over the past several years, we have been investigating small, lead-like natural products of the tropolonoid families such as hinokitiol (HKT or  $\beta$ -thujaplicin). This simple monoterpene is produced by a variety of plant species and has shown anti-proliferative activity against both bacterial pathogens and select malignant cells as well as insecticidal and antifungal effects.<sup>4-6</sup> Central to the structure of these secondary metabolites is a fully conjugated  $\alpha$ -hydroxyketone system that endows this group with properties of both a carboxylic acid (readily ionizeable at physiological pH) and a hydroxamic acid (ability to form strong five-membered metal chelates), thus providing multiple modes for potential target interactions (Figure 1).

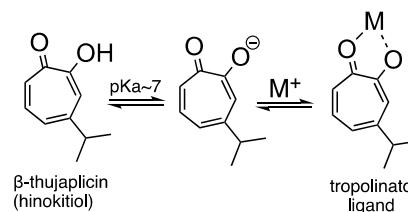


**Figure 1.** The natural product hinokitiol (HKT or  $\beta$ -thujaplicin) and key species involved in targeting metalloenzymes.

We view these small terpenes as more lead-like than typical natural products, being rule of 3-compliant,<sup>7</sup> having multiple positions readily available for synthetic elaboration and a propensity to demonstrate moderate activity against a variety of targets.<sup>8,9</sup> We were aware of reports regarding the antibacterial activity of HKT against the Gram-negative organism *Escherichia coli*.<sup>10</sup> and evaluation of several synthetic tropolones showed promising levels of antibacterial activity. Encouraged by these results, we proceeded to explore potential targets using an unbiased target identification approach. These studies reveal that bacterial enolase, an essential metalloenzyme involved in a range of cellular functions, is inhibited by several synthetic tropolones as well as related troponoid structures. Supported by crystallographic and modelling experiments with the enzyme derived from *E. coli*, this study has

delivered a lead series for further development against this essential, yet unexplored, bacterial target.

## MATERIAL AND METHODS

**Reagents.** D-(+)-2-Phosphoglyceric acid sodium salt was purchased from Santa Cruz Biotechnology, Inc. The enolase positive control from Baker's yeast (*S. cerevisiae*) was purchased from Sigma-Aldrich. AP-III-a4 (ENOblock) was purchased from Selleckchem. Thrombin CleanCleave kit (RECOMT) was purchased from Sigma-Aldrich.

**DARTS procedure.** A cryogenically stored sample of *E. coli* 25922 was plated on a LB agar plate and incubated at 37°C overnight. From the culture plate a single colony was picked using a sterile loop and added to 20 mL of LB media in a sterile 50 mL Falcon™ conical tube. The tube was incubated at 37°C and shaken at 225 rpm in a New Brunswick Scientific C25KC incubator shaker overnight. 15 mL of culture was diluted with 10 mL of fresh LB media and OD<sub>600</sub> was read on a Shimadzu BioSpec-mini. 4 mL of diluted culture was added to each well of a 6-well plate. Appropriate amounts of either DMSO or tropolone were added to each well with less than 4% DMSO in the final volume. The 6-well plate was then incubated at 37°C overnight. The resulting bacterial culture from each well was transferred to separate 1.5 mL Eppendorf tubes and centrifuged at 14,000 rpm for 3 minutes. The supernatant was discarded, and the process repeated until all culture had been pelleted. Pellets were then washed with phosphate buffered saline and centrifuged at 14,000 rpm for 3 minutes. Supernatant was discarded, and the pellet was broken up by mechanical agitation. Next, 200 µL of bacterial protein extraction reagent (B-PER) with 2 µL of Halt Protease and Phosphatase Inhibitor Cocktail were added to lyse the cells. The lysate was placed on a rocker at 4°C for 45 minutes and then centrifuged at 14,000 rpm for 15 minutes. After centrifuging, the supernatant was transferred to a new 1.5 mL Eppendorf tube and mixed with 200 µL of DARTS assay buffer and placed on ice. DARTS assay buffer was previously prepared in an autoclaved 100 mL bottle by mixing Tris-HCl (50 mM), sodium chloride (50 mM) and calcium chloride (10 mM) in sterilized, filtered water. The protein content in each tube was measured using the Bradford Assay and 1 µg of thermolysin (from Promega) was added for every 15 µg of protein reported. Since the amount of thermolysin required was significantly less than 1 mg, 1 mM stock of thermolysin was prepared in sterilized, filtered water. The samples were then incubated at room temperature for 10 minutes. Proteolysis by thermolysin was quenched by adding 0.5 M EDTA in a 1:10 volumetric ratio (20 µL). Samples were stained with NuPAGE and run on a 4-12% Bis-Tris gel at 184 volts. After cooling, the gel was stained with Coomassie blue. Gel images were recorded using a Nokia Lumia 920. The differential band was excised from the gel using a sterile razor blade and sterile tweezers and placed in 500 µL of sterilized, filtered water in a sterile 1.5 mL Eppendorf tube. The tube was sealed with parafilm and shipped via FedEx to the Keck MS & Proteomics Resource at Yale School of Medicine for LC-MS/MS protein identification.

**Cloning and expression of recombinant *E. coli* enolase.** The *E. coli* enolase gene (UniProtKB: P0A6P9) was synthesized and cloned in the pET-28a(+) vector with a N-terminal cleavable His<sub>6</sub> tag via BamHI and EcoRI restriction sites by GeneScript.

A single colony of BL21(DE3) (Novagen) transformed with the plasmid was incubated in 50 mL of LB media containing 30 µg/mL kanamycin, at 37°C for 12-14 h shaking at 225 rpm. The cell culture was diluted to 0.05 OD<sub>600</sub> in freshly prepared LB with 30 µg/mL kanamycin and incubation continued until an OD<sub>600</sub> reading of 0.7-0.8. The temperature was reduced to 30 °C and expression was induced with 1 mM isopropyl-β-D-thiogalactopyranoside (IPTG).

After 6 h incubation the cells were harvested by centrifugation; the cell pellets were flash frozen in liquid nitrogen and stored at -80 °C

**Purification of recombinant His-tagged enolase.** Cell pellets were thawed and resuspended with Lysis Buffer comprising 50 mM Tris pH 8.0, 0.4 M NaCl, 5 mM β-mercaptoethanol and 200 µg/mL lysozyme. One tablet of EDTA-free protease inhibitor (Roche Applied Science) was added per 10 mL of cell lysis buffer. After 20 min incubation on ice the cell suspension was disrupted by sonication (Qsonica 125 Ultrasonic Processor). Cell debris was removed by centrifugation at 20K x g for 25 minutes. The soluble lysate was filtered with a 0.45µm filter and added to a nickel column (PerfectPro matrices) equilibrated with buffer A (50 mM Tris pH 8.0, 0.4 M NaCl, 5 mM imidazole and 5 mM MgCl<sub>2</sub>). Protein was eluted with buffer A supplemented with 250 mM imidazole. Fractions containing enolase were identified by SDS-PAGE gel, pooled and concentrated using a Centricon filter unit (Millipore). The protein sample was then subjected to a HiPrep 26/60 Sephacryl S-200 column (GE Healthcare) equilibrated with 25 mM Tris pH 7.5, 100 mM NaCl, 5 mM MgCl<sub>2</sub> and 0.5 mM DTT. The predominant protein peak eluted with an apparent molecular weight of 93 kDa which is consistent with the native molecular weight of dimeric *E. coli* enolase (91.2 kDa). Appropriate fractions were pooled, concentrated to 8.0 mg/mL, flash frozen with liquid nitrogen and stored at -80 °C. The high level of protein purity was confirmed by SDS-PAGE stained with Coomassie Blue.

**Removal of the N-terminal polyhistidine tag by thrombin treatment.** The N-terminal fusion partner of His-Eno was removed by incubation of the purified recombinant protein with thrombin-agarose suspension at 4 °C for 24 h. After cleavage, the protein mixture was removed by centrifugation for 5 min at 500g. Following the absorption with an equal amount of 50% Ni-NTA agarose slurry, (Qiagen, USA) for 30 min at 4 °C, the untagged target protein was recovered with the flow-through, whereas the his-tagged protein remained bound to the column. The flow-through was buffer exchanged into 25 mM Tris-HCl, 100 mM NaCl and 2 mM MgCl<sub>2</sub> buffer (pH 8.0). SDS-PAGE analysis was used to confirm the efficient removal of the N-terminal fusion and almost complete recovery of the detagged sample.

**Enolase activity and inhibition assay.** The activity of recombinant tagged and untagged enolase was determined by direct monitoring of the increase in PEP absorbance at 240 nm, using DU 640 spectrophotometer (Beckman). The standard assay contained 50 mM Tris pH 8.0, 0.1 M KCl, 0.5 mM 2-phosphoglycerate (as the glycolysis substrate) and 1 mM MgSO<sub>4</sub> because of its importance in stabilizing dimer contacts. The reactions were carried out at 25 °C, at a final volume of 500 µL. One unit of enolase activity was defined as the amount of protein which catalyzes the formation of 1µmole PEP from 2-PGA in 1 minute under these standard conditions. The concentration of PEP was determined using a molar extinction coefficient ( $\epsilon_{240\text{ nm}} = 1,300\text{ M}^{-1}\text{ cm}^{-1}$ ).

Inhibition of enolase activity by tropolones was performed at a constant enolase concentration of 40 nM and inhibitor concentrations close to the MICs values. The compounds supplied in 50 mM Tris pH 8.0 and 5% DMSO were preincubated with the protein sample for 5 minutes in the assay buffer consisting of 50 mM Tris pH 8.0, 0.1 M KCl and 1 mM MgSO<sub>4</sub>. The reaction was initiated by the addition of 2-PGA substrate at 1.0 mM final concentration. The decrease in enolase activity upon inhibition was monitored at 15 second intervals for a period of 4 minutes at 240 nm. The measurements were repeated and the average half maximal inhibitory concentrations (IC<sub>50</sub>) were calculated from initial rates of absorbance increase. Baker's yeast enolase (Sigma-Aldrich) served as a positive control in the assay.

The binding response of the five key tropolone derivatives at fixed concentration of substrate (1 mM) and four inhibitor concentrations

(1  $\mu$ M, 5  $\mu$ M, 10  $\mu$ M, and 20  $\mu$ M) was performed to determine the half maximal inhibitory concentration ( $IC_{50}$ ) of the tropolones. This data is summarized in Supporting Information (Table S1).

**Isothermal Titration Calorimetry.** ITC measurements were carried out at 25°C using a Nano-ITC instrument (TA instrument) with stirring at 300 rpm. Tagged protein sample in 25 mM Tris buffer pH 7.5, 75 mM NaCl, 5 mM  $MgCl_2$  and 1 mM DTT was dialyzed overnight into 1 L of 20 mM Hepes 7.5, 50 mM NaCl, 1 mM  $MgCl_2$  and 0.8 % DMSO. Protein and ligand concentration (compound **10**) were adjusted to 90  $\mu$ M and 800  $\mu$ M, respectively with the dialysis buffer and degassed for 5 minutes prior to usage. Aliquot (2.5  $\mu$ L) of the ligand was injected into the protein sample until binding appeared saturated (20 injections, at 300 s intervals). Titrations of ligand buffer-only sample was performed to provide baseline readings. The corrected heat change was fitted with an independent binding model in the NanoAnalyze software (TA instrument) to obtain binding affinity constants ( $K_d$ ), enthalpy and entropy of binding ( $\Delta H$  and  $\Delta S$ ) as well as the stoichiometry ( $n$ ) of binding

**Differential scanning calorimetry (DSC).** Prior to the analysis the protein sample was buffer exchanged into 20 mM HEPES (pH 7.0), 50 mM NaCl and 2 mM  $MgCl_2$ . The concentration of protein and ligand were adjusted to 6  $\mu$ M and 60  $\mu$ M, respectively. Purified enolase with and without ligands were heated at 1 °C/min, starting at 0 °C and up to 120 °C using a NanoDSC instrument (TA instruments). The samples were degassed extensively prior to injection into the calorimeter cell in order to prevent formation of air bubbles. The reference cell was filled with buffer for all runs. A pressure of 3atm was applied to both cells during the run. The excess heat capacity scans for the protein transitions were obtained by subtracting a control scan of buffer versus buffer. The data were corrected for the difference in heat capacity between the initial and the final state by using a sigmoid baseline in the NanoAnalyze software (TA instruments) and a two-state transition model was used to determine the  $T_m$  and  $\Delta H$  values.

**Protein crystallization.** Crystal Screen 1 and 2 (Hampton Research) were applied to purified cleaved and uncleaved form of the enolase. Only Condition 14 from Crystal Screen 2 (2.0 M ammonium sulfate, 0.1 M Sodium citrate tribasic dihydrate at pH 5.6 and 0.2 M Potassium sodium tartrate tetrahydrate) produced small irregular shape crystals of the detagged enzyme that were further optimized. For setups, 2  $\mu$ L of protein (at 10–15 mg/mL in 25 mM Tris pH 7.0, 100 mM NaCl, 5 mM  $MgCl_2$  and 1 mM DTT) was mixed with 2  $\mu$ L of optimized crystallization solution (2.0 M ammonium sulfate, 0.1 M MES at pH 6.0, and 0.1M Na/K Tartrate) at 20 °C using hanging drop method. Large crystals grew within 3-4 days. Both co-crystallization and soaking methods were used to obtain the substrate-bound enolase crystals. The cleaved protein (12 mg/mL) was incubated with 2-PGA for 2 h on ice. An equal volume of the protein-ligand complex was then mixed with a reservoir solution and left at 20 °C for a few days. Crystals prepared for soaking were initially grown in the optimized ammonium sulfate condition. The 2.5 mM (final concentration) substrate was then added to the drops containing large crystals and soaked overnight. For freezing, crystals were either transferred to a cryosolution containing 25% (v/v) glycerol, 2.0 mM ligand and 15 mM  $MgCl_2$  or 2.5 M Lithium Sulfate and flash cooled with liquid nitrogen and the high-resolution data sets were collected remotely at SSRL on beamline 14-1.

**Structure determination of a 2-PGA: ecEnolase complex.** The first dataset was collected on *E. coli* enolase co-crystallized with 2-PGA and cryo-protected in 2.5 M lithium sulfate, at Brookhaven National Laboratories synchrotron facility NSLS-II, on beam line 17-ID-1 (AMX), using an Eiger9M pixel-array detector. Images were processed at the beam line using XDS.<sup>11</sup> The crystal diffracted to 2.2Å in space group  $P2_12_12_1$  with unit cell parameters:  $a=111.26\text{\AA}$ ,  $b=143.29\text{\AA}$ ,  $c=207.04\text{\AA}$ .

A second data set was later collected on enolase co-crystallized with 2-PGA, where the crystal was cryo-protected with glycerol and back-soaked in 2-PGA and MgCl<sub>2</sub>, before being flash-frozen for data collection. Data collection was performed remotely at beam line 14-1 at the Stanford Synchrotron Radiation Laboratory (SSRL), using a Rayonix MX325 CCD detector. Images were processed in CCP4i2 using iMosflm.<sup>12,13</sup> The crystal diffracted to 1.8Å in space group P2<sub>1</sub>2<sub>1</sub>2<sub>1</sub> with unit cell parameters: a=105.94Å, b=142.40Å, c=206.64Å.

Molecular replacement was performed with the CCP4i2 (PHASER) software using the 2FYM structure of *E. coli* enolase complexed with a minimal binding segment of RNase E for both enolase datasets.<sup>27</sup> Six molecules (three dimers) were found in the asymmetric unit. Rebuilding and refinement were done in CCP4i2, using COOT) and Refmac5 respectively, for both datasets.<sup>14,15</sup> The dataset that was not back-soaked contained one apo-enolase dimer, and two dimers with substrate (one monomer has a mix of substrate (2-PGA) and product (PEP)). The back-soaked 1.8Å dataset has one well-defined 2-PGA molecule as well as 2 Mg-ions in all six active sites for the three dimers, and thus we denote this as a substrate-bound structure. Data collection, refinement and structure statistics for both structures are summarized in Supporting Information (Table S5).

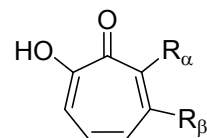
**Docking analysis.** Molecular modeling was carried out using Schrödinger Small-Molecule Drug Discovery and Biologics Suites. The crystal structure of *E. coli* enolase (PDB 6BFZ) co-crystallized with 2-PGA and determined herein was used. The structure was prepared for docking using the Schrödinger Protein Preparation Wizard.<sup>16</sup> Missing hydrogen atoms were added, het states were generated using Epik with pH 7.0 ± 2.0 and zero-order bonds to metals created, followed by the generation of metal binding states.<sup>16</sup> Sample water orientations using PROPKA with pH 7.0, waters less than 3 H-bonds to non-waters were removed and the protein was minimized using OPLS3 to converge heavy atoms to an RMSD of 0.3 Å.<sup>17</sup>

The active site was defined using the receptor grid generation tool by picking the residues (D316, K392, Q166, S41 and D245) around the Mg<sup>2+</sup> ion. Ligands with length less than or equal to 15 Å was allowed for docking. Metal coordination constraint was selected in the grid generation. All other parameters were used as is. All compounds were constructed using Maestro's building tool and energetically minimized, LigPrep was used to generate different ionization states at pH 7.0 ± 2.0 using Epik.<sup>18</sup> The ligands were desalted and different tautomers were generated. All dockings were carried out using Glide SP (version 7.7) and all other parameters kept with the default values.<sup>19</sup>

## RESULTS AND DISCUSSION

We evaluated the antibacterial activity of  $\alpha$ - and  $\beta$ - substituted tropolones, using a growth inhibition assay with four priority Gram-negative pathogens. The panel included two members of the Enterobacteriaceae family, *E. coli* and *Klebsiella pneumoniae* (Kp) as well as the very challenging organisms *Acinetobacter baumannii* (Ab) and *Pseudomonas aeruginosa* (Pa). Several tropolones exhibited activity against all four pathogens with the most potent minimum inhibitory concentration (MIC) values between 10-14  $\mu$ g/mL (Table 1). Notably, small structural changes relative to the natural product HKT (**9**) both increased potency and expanded coverage. Analogs **1**, **2** and **13** were of particular interest as they displayed the best activity against *P. aeruginosa* where the MIC was equal or only two-fold higher than that for the other species. The importance of the anionic nature of the metal binding moiety was underscored by the complete abrogation of antibiotic activity upon methylation of HKT to give ether **15**.

**Table 1. MIC values ( $\mu$ g/mL) for selected tropolone derivatives<sup>a</sup> against Gram-negative bacteria**



ID	R $\alpha$	R $\beta$	MIC (Kp)	MIC (Ec)	MIC (Ab)	MIC (Pa)
1		H	19.8	19.8	19.8	19.8
2		H	13.8	13.8	13.8	27.7
3		H	19.0	19.0	19.0	38.0
4		H	11.3	22.6	22.6	45.2
5		H	18.8	18.8	18.8	>1000
6		H	24.0	24.0	24.0	48.0
7		H	25.0	25.0	25.0	50.0
8		H	25.6	25.6	25.6	51.2
9	H		31.2	25	10	>164
10	H		31.2	20	10	>40
11	H		12.0	23.8	12.0	95.0
12	H		11.4	22.3	11.4	44.5
13	H		11.4	22.3	11.4	22.3
14	H		>1000	>1000	>1000	>1000
15			>500	>500	>500	>500

<sup>a</sup> Substituted tropolones exist as a mixture of tautomers. The non-ionized  $\alpha$ - and  $\beta$ -tropolones are depicted as a single tautomer for clarity. At physiological pH, tropolones are ionized and resonance renders the two oxygen atoms equivalent.

As previous studies to examine the mechanism of antibacterial action of tropolones have been limited, including their effect on cellular morphology, we used confocal microscopy of Gram-stained preparations of *E. coli* cells treated with various compounds (Figure 2).<sup>6</sup> Images of the untreated cells (Figure 2a) and cells treated with the O-methylated tropolone (Fig. 2b) show little difference in morphology. However, images after treating the cells with 20  $\mu$ g/mL of either HKT or synthetic compound **2** (Fig. 2c, 2d) show that the cells become filamentous, with some cells extended by ~6-16-cell lengths, suggesting incomplete cell division. These observations strongly imply that the tropolones may be impacting cell wall biosynthesis or inhibiting targets critical for cell division.

1  
2  
3  
4  
5  
6  
7  
8  
9  
10  
11  
12  
13  
14  
15  
16  
17  
18  
19  
20  
21  
22  
23  
24  
25  
26  
27  
28  
29  
30  
31  
32  
33  
34  
35  
36  
37  
38  
39  
40  
41  
42  
43  
44  
45  
46  
47  
48  
49  
50  
51  
52  
53  
54  
55  
56  
57  
58  
59  
60

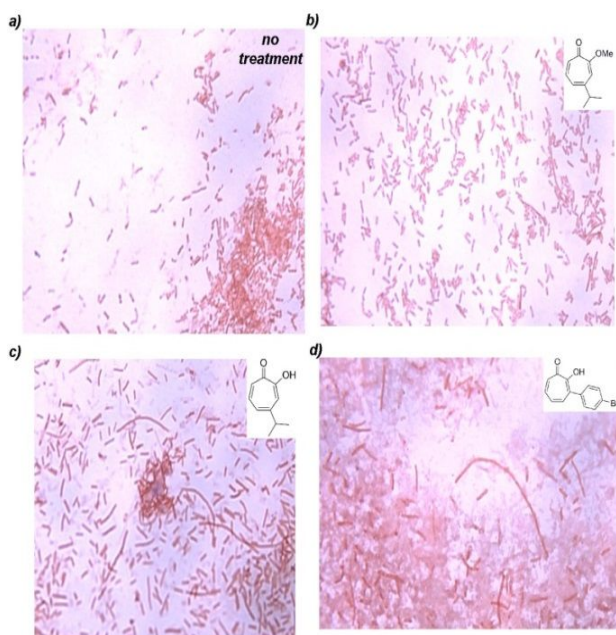


**Figure 2.** *E. coli* cells treated with a) DMSO, b) methylated HKT as a negative control, compound **15**, c) HKT, d) compound **2**

### IDENTIFICATION OF ENOLASE AS A POTENTIAL TARGET FOR TROPOLONES

A variety of potential bacterial targets for tropolones have been suggested including CapF, tyrosinase, and elastase.<sup>20–22</sup> As these tropolone compounds are more indicative of early leads, there is a strong likelihood that they can exert cellular activity through multiple targets. We chose an unbiased approach to target identification to probe any additional opportunities for lead development. We utilized the drug affinity responsive target stability (DARTS) method, a relatively new technology for direct target identification.<sup>23,24</sup> Briefly, cell lysates are pre-incubated with the compound of interest and subjected to limited proteolysis with the notion that bound complexes will be protected due to their compact, folded nature. These protected proteins persist on a protein gel when compared to untreated controls. The first reports of the use of DARTS originated in mammalian cells and identified translation initiation factor 4A (eIF4A) as a potential target of resveratrol.<sup>23</sup> Here, we slightly modified the DARTS protocol to adapt and optimize it for the target identification in bacterial/prokaryotic cells. Upon treatment of *E. coli* cell lysate with compound **5** one band persisted in the treated lane (Figure 3). Mass spectrometry analysis determined that this band corresponds to enolase with 83 % coverage. The identification of enolase is compelling as it is a known, essential enzyme that reversibly converts 2-phosphoglycerate (2-PGA) to phosphoenolpyruvate (PEP) as a key step in glycolysis is an indispensable component of the glycolytic machinery, inhibition of enolase would be expected to have significant effects on cell growth as illustrated by experiments with conditional knock-outs of enolase in *S. aureus*.<sup>25</sup> Moreover, the product of enolase, PEP, is a critical structural component of the bacterial cell wall where it provides the linker between the glycan and peptide domains of the peptidoglycan layer. PEP acts as a substrate for MurA in the first committed step of cell wall biosynthesis.

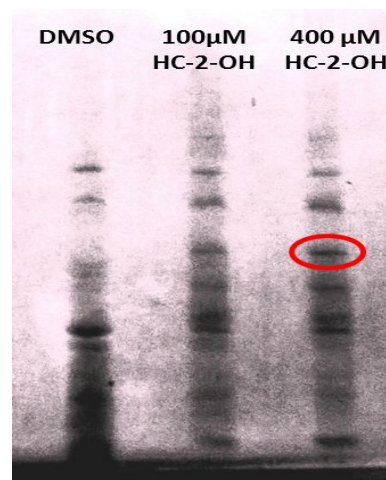
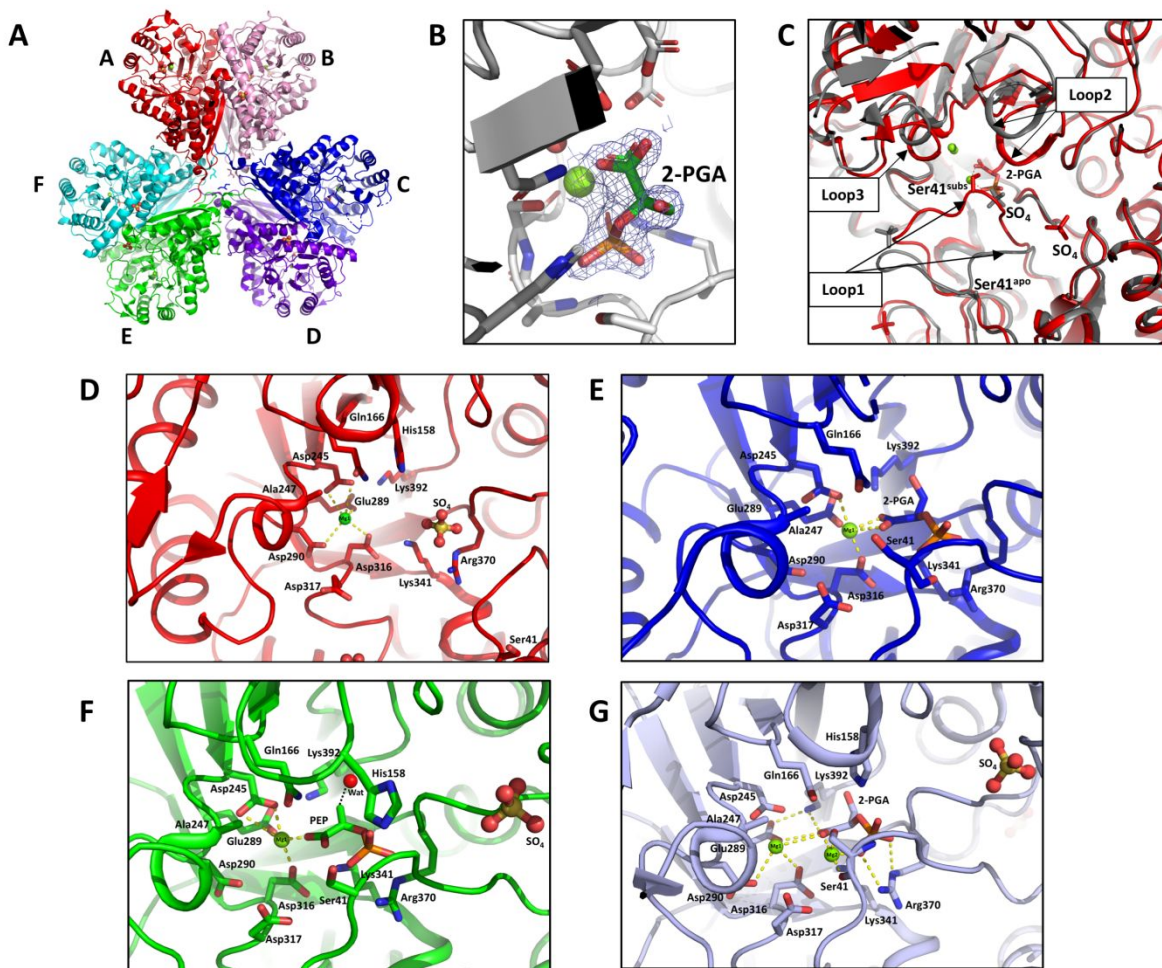


**Figure 3.** DART analysis of *E. coli* lysate treated with compound **5**.

The clinical agent fosfomycin targets MurA and it was shown that genetic knock-out of enolase potentiated the effect of fosfomycin.<sup>26</sup> Enolase behaves as a ‘moonlighting’ enzyme, playing an additional role in the RNA degradosome where it forms a complex with RNaseE, RhlB and PNPase to degrade mRNA in the cell.<sup>27</sup> The role of enolase in the degradosome may be related to the specific degradation of mRNAs coding for glucose transporters, especially under metabolic stress. The degradosome has also been shown to be part of the bacterial cytoskeleton that play an important role in cell wall formation and division.<sup>28</sup> It is noteworthy that enolase is a metalloenzyme and would be presumed to be a promising target for leads containing metal chelating pharmacophores. Alignment of the amino acid sequences of *E. coli* enolase, human counterparts and other eukaryotic and prokaryotic enolases reveal a conserved constellation of active site residues and two  $Mg^{2+}$  ions involved in the ligand binding, suggesting a common mechanism for the metal-dependent activity.<sup>29–31</sup> The importance of the metal binding motif and backbone constituents needs to be, therefore, carefully considered in the context of the full structure of the target enzyme and not just an active site when optimizing for potency and selectivity. There is comparatively little structural information regarding prokaryotic enolases to assist in structure-based drug design efforts, especially complexes with substrates or inhibitors. As an important first step in exploring enolase inhibition as an antibacterial strategy, we set out to secure high-resolution crystal structure of the enolase from *E. coli*.

### STRUCTURE DETERMINATION

To better understand the active site architecture of *E. coli* enolase we generated two crystal structures of enolase in complex with the 2-PGA substrate (Figure 4). In the first structure, obtained from a crystal that was frozen in 20% glycerol without adding additional 2-PGA or Mg upon soaking, the enzyme adopts three distinct catalytic site states (PDB ID: 6BFZ). Three dimers form a hexameric complex with one dimer in its Apo-form (chain A, B), the second dimer with 2-PGA bound (chain C, D) and the third dimer with 2-PGA bound in one monomer (chain F) and a mixed population of substrate and product (2-PGA and PEP plus a water molecule) at half occupancy in the second monomer (chain E). In the second structure, obtained after freezing the crystal in a cryo-solution that was supplemented with 2mM 2-PGA substrate and 5 mM  $MgCl_2$ , we observe a fully occupied active site with 2-PGA and two  $Mg$ -ions bound (PDB 6BFY) (Figure 4).

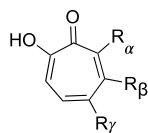


**Figure 4.** (A) Overall structure of *E. coli* enolase complexed with substrate 2-PGA (PDB ID: 6BFY). Three dimers form a hexameric complex through interaction of the N-terminal T7-tag. (B)  $2F_o - F_c$  electron density of 2-PGA and Mg (II) in the 1.8 Å structure (6BFY) contoured at 2 sigma. (C) Superposition of Chain A (apo-enolase) from 2.2 Å structure (PDB ID: 6BFZ) with 2-PGA-bound enolase (PDB ID: 6BFY). Large conformational changes are seen in three main regions; Loop1 (residues 37-47), Loop2 (residues 151-167) and Loop3 (residues 245-271). (D) The crystal structure of the active site of *E. coli* enolase (PDB 6BFZ) apo-form (Chain A), (E) with 2-PGA substrate (Chain C) (Chain E active site contains a mix between substrate and product, but only the PEP product is shown for clarity). (G) The active site in chain A of PDB 6BFY is fully occupied with 2-PGA substrate as well as two Mg<sup>2+</sup>-ions.

Analysis of the substrate-bound enolase crystal structure shows that the active site undergoes significant changes compared to the apo-form upon binding the substrate (Figure 4C). The Ser41 residue in Loop1 moves closer to the phosphate group of the substrate and directly interacts with the second Mg<sup>2+</sup>-ion (Mg2) (Figure 4D versus 4G). The distance between Mg1 and Ser41 is 6.8 Å in the substrate-bound (PDB 6BFY) compared to 17.2 Å in the apo-form (PDB 6BFZ) (Figures 4D, G). The shorter distance in the substrate-bound structure is the result of the coordination of Ser41 to the second Mg<sup>2+</sup> ion (Mg2). Finally, analysis of the product-bound structure (in molecule E, where there is a mix of substrate and product) shows the distance between Mg1 and Ser41 to be 9.2 Å (Figure 4F) and reveals no interactions between the phosphate group and Ser41. Two other loop regions undergo significant rearrangements upon substrate binding; Loop 2 (residues 151-167) and Loop 3 (residues 245-271).

## ENZYME INHIBITION STUDIES

We expressed, purified, and crystallized the recombinant N-terminal cleavable His-tagged *E. coli* enolase (His-Eno) in order to perform enzyme assays and probe structure-activity relationships. Enolase inhibition was measured spectroscopically by monitoring the formation of PEP from 2-PGA at 240 nm. Using this reaction and a high fixed concentration of compounds (50 μM), we first measured the inhibition of the tagged enolase by three tropolones from the initial antibacterial screen and six compounds with alternative metal-binding motifs to evaluate the specificity of inhibition by tropolones (Supporting material, Table S2). From this group, the tropolone derivatives were the most potent, with inhibitory activity ranging from 53% to 78% and appeared better suited for inhibition compared to alternative chelation motifs.

**Table 2. Inhibition of *E. coli* Enolase by Tropolone Derivatives at 20  $\mu$ M Concentration**

Compound	R $\alpha$	R $\beta$	R $\gamma$	% Inhibition	Compound	R $\alpha$	R $\beta$	R $\gamma$	% Inhibition
2		H	H	70%	29		H	H	70%
17		H	H	52%	30		H	H	28%
18		H	H	32%	31		H	H	35%
19		H	H	61%	32		H	H	7%
20		H	H	31%	9	H		H	55%
1		H	H	33%	10	H		H	72%
21		H	H	20%	12	H		H	66%
22		H	H	30%	13	H		H	24%
23		H	H	13%	11	H		H	19%
24		H	H	16%	37	H	H	NH <sub>2</sub>	19%
25		H	H	13%	38	H	H		53%
26		H	H	8%	39	H	H		15%
27		H	H	58%	40		H	H	72%
28		H	H	35%	41	ENOblock			41%

Preliminary SAR data was generated by expanding enzyme inhibition screening to a larger collection from our tropolone library containing ~25 positional isomers of mono-substituted derivatives. Screening of the compounds at a fixed concentration of 20  $\mu$ M revealed a significant role for the side chain substitutions on enolase activity (Table 2).

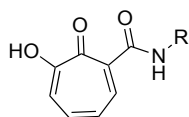
In general, inhibitory activity was observed for compounds from each of the three different mono-substitution classes. A strong influence from the pendant sidechain group was noted as well, yielding inhibition values in a broad range from 7-72% at 20  $\mu$ M. Both aromatic and linear branched substituent at the  $\alpha$ - or  $\beta$ -position were associated with stronger inhibition (e.g.  $\alpha$ -bromophenyl **2**,  $\alpha$ -pentyl **29**,  $\beta$ -Ph **10**). More extensive

branching from the aryl ring greatly reduced inhibition (e.g. alkynyl **22-23** or acetamide **32** at the  $p$ -position). Introduction of polar functionality on the peripheral group as with morpholine (**19**) to balance some of the overall hydrophobic character of the inhibitors could be achieved while maintaining reasonable potency. Interestingly, while the  $\gamma$ -amino derivative (**37**) showed weak activity, acetylation with a branched amide (**38**) improved activity while linear substitution (**39**) was deleterious. Indeed, docking experiments with compound **2** and **10** suggest a possible steric clash posed by the longer linear substituent at  $\gamma$ -position with the active site residues, His158 and Glu208 (Figure 5). The known mammalian triazine enolase inhibitor enoblock (**41**) was also included in our studies and its effect measured against

the *E. coli* enolase at 10  $\mu\text{M}$  and 20  $\mu\text{M}$  concentration.<sup>32,33</sup> Although it showed moderate inhibitory activity with 28% and 41% inhibition at 10 and 20  $\mu\text{M}$  concentration, respectively, these values are two-fold lower than the values obtained for the best tropolones.

To further investigate the effect of additional chelating functionality, a small library of novel tropolones with a carboxamide moiety at the  $\alpha$ -position of tropolone was prepared. This new series introduces additional functional groups that can form H-bonding and a possibility to coordinate with an additional  $\text{Mg}^{2+}$  ion in the enzyme pocket. When screened at 20  $\mu\text{M}$  concentration (Table 3), these compounds showed similar level of activity, between 44% and 71%, across different substituents. This suggests that additional chelating group is poorly disposed/oriented to interact with the second  $\text{Mg}^{2+}$  ion in the active site.

**Table 3. Inhibition of *E. coli* Enolase by Acyltropolone Derivatives at 20  $\mu\text{M}$  Concentration**



ID	R	% Inhibition
40		63%
41		55%
42		44%
43		71%
44		68%

Utilizing an unbiased target-identification approach, we determined that both the naturally occurring  $\beta$ -thujaplicin and related synthetic tropolones can inhibit the function of the essential bacterial enzyme enolase in the low micromolar range. This level of enzymatic inhibition of selected  $\alpha$ - and  $\beta$ -substituted tropolones is reasonably correlated to the antibacterial effects on the growth of live bacteria across four different pathogens however, the contribution of other target inhibition by these early leads cannot be excluded. Additional biophysical studies on the association between enolase and lead tropolones were conducted to elucidate the interactions.

## ISOTHERMAL TITRATION AND DIFFERENTIAL SCANNING CALORIMETRY

To establish binding efficiency and the energetics of enolase-tropolone interactions, ITC analysis were carried out using a Nano-ITC instrument (TA instrument). Control experiment involved titration of dialysis buffer with 800  $\mu\text{M}$  compound **10** to provide baseline reading. The heat burst generated after addition of the ligand to the solution containing 90  $\mu\text{M}$  enzyme were corrected and fitted with an independent binding model. The ITC profile and the thermodynamic parameters related to the binding are shown in Supporting Information (Figure S3). The binding affinity of compound **10** to enolase ( $K_d$ ) was  $1.43 \pm 0.23 \mu\text{M}$ , in a reaction driven by unfavorable enthalpy changes ( $\Delta H = 2.59 \pm 0.15 \text{ kcal/mol}$ ). The binding entropy was found to be a favorable, positive value ( $T\Delta S = 10.57 \pm 0.18 \text{ kcal/mol}$ ). The observed free energy ( $\Delta G$ ) was calculated using the thermodynamic standard Gibb's equation  $\Delta G = \Delta H - T\Delta S$  and was found to be  $-7.98 \text{ kcal/mol}$ . The stoichiometry of the binding was calculated from fitting of the binding isotherm which gave the value of  $n = 1.05 \pm 0.14$  suggesting 1:1 stoichiometry of the enolase: ligand complex.

Binding of ligand to a protein is known to increase its thermal stability and cause a shift between the thermal denaturation curves of the unliganded versus liganded protein. To determine the capacity of purified recombinant enolase to bind tropolones and gain insight into the potential druggability of the binding site, we examined thermal stability of enolase using a NanoDSC instrument (TA instruments). The excess heat capacity scans for the protein transitions were obtained by subtracting a control scan of buffer versus buffer containing tested ligand. In the absence of tropolone, enolase (6  $\mu\text{M}$ ) showed thermal denaturation at 53.7  $^{\circ}\text{C}$ . Treatment with 60  $\mu\text{M}$  Compound **10** and Compound **2** resulted in a shift of 4  $^{\circ}\text{C}$  and 3.1  $^{\circ}\text{C}$ , respectively (Supporting Information, Figure S4). This increase in  $T_m$  ( $\Delta T_m$ ) is an indication of stabilization upon tropolone binding to enolase that correlates well with the  $\text{IC}_{50}$  at low micromolar range.

## DOCKING OF TROPOLONES TO ENOLASE

Initial attempts to dock tropolones on the structure of enolase in complex with the 2-PGA substrate were ambiguous. Our prior structural analysis rationalizes the difficulty in producing docked structures to this form of the enzyme due to the restricted nature of the substrate-bound structure (closing due to conformational changes in Loop 1-3). That lead us to carry out molecular docking using the apo-form of the enzyme (Molecule A of PDB ID: 6BFZ). Three tropolone derivatives with different inhibitory activity against enolase were chosen from Table 2. The docking of **1** to the active site shows that this molecule forms an asymmetric bi-dentate interaction with  $\text{Mg}1$  with a distance of 2.0  $\text{\AA}$  and 2.6  $\text{\AA}$ . It also interacts with the residues Asp316, Asp317, Asp245 and Gln166 (Figure 5A). Compound **2** interacts with  $\text{Mg}1$  through a monodentate interaction (2.1  $\text{\AA}$ ) and is rotated by 180 degrees (Figure 5B). Compound **10** (a beta-substituted tropolone) binds similarly to Compound **2**, but interestingly forms an asymmetric bi-dentate interaction to  $\text{Mg}1$  (2.0  $\text{\AA}$  and 3.3  $\text{\AA}$ ) (Figure 5C). Compound **43**, of the second series of tropolones (Table 3), is predicted to interact in a tight bi-dentate manner with  $\text{Mg}1$  (2.1  $\text{\AA}$  and 2.3  $\text{\AA}$ ) and to form close interactions between the amide carbonyl oxygen and Lys341, as well as Asp317 and Asp245.

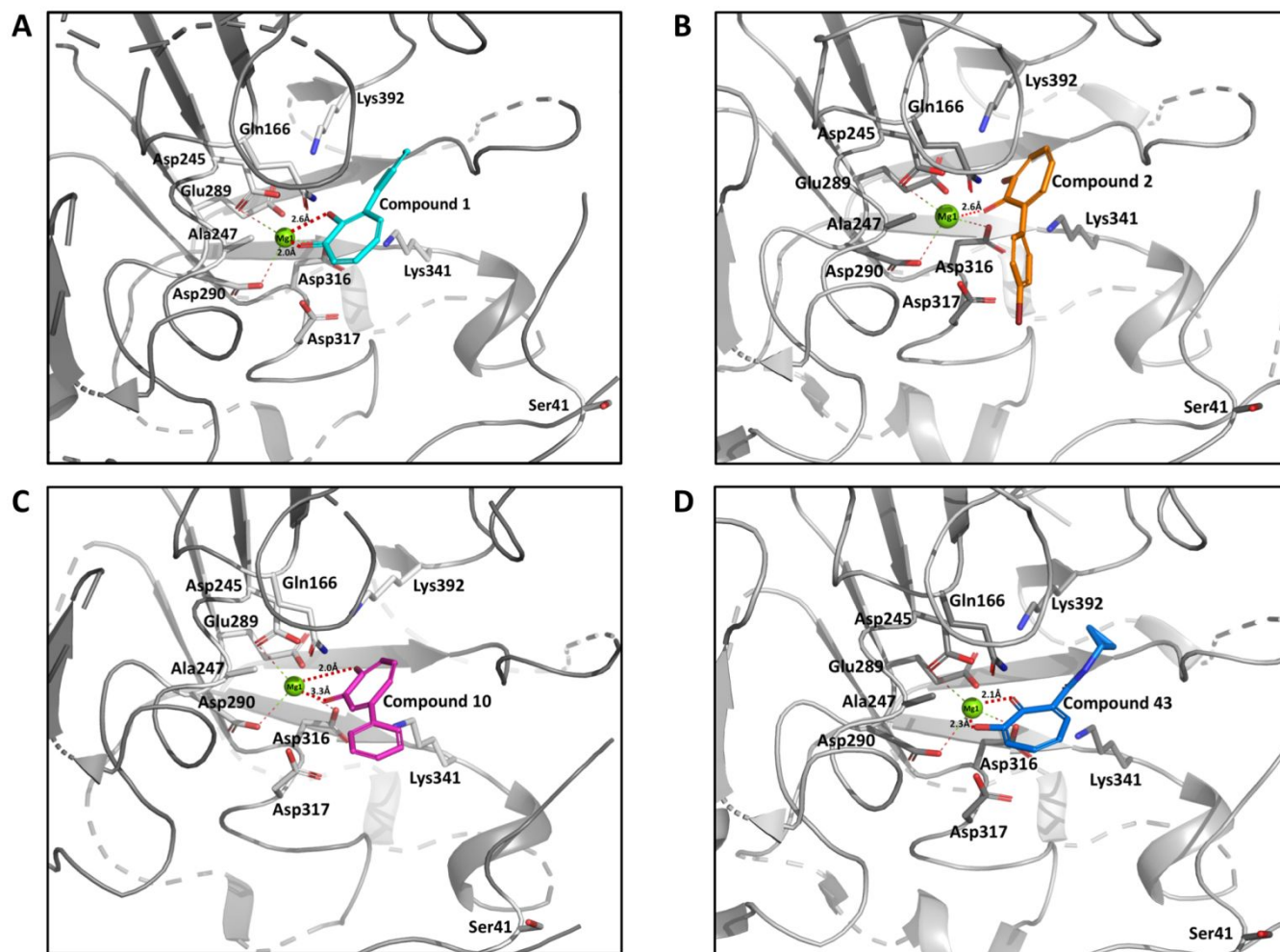


**Figure 5:** Binding poses of the tropolone derivatives. (a) Compound 1, (b) 2, (c) 10 and (d) 43. Compounds are shown in different colored sticks. Oxygen is colored red and nitrogen is colored blue. Interactions between the compound and Mg1 are shown as dotted lines.

## CONCLUSION

In summary, DARTS assay has been used to identify enolase as a potential drug target. A series of tropolone derivatives, designed to target this crucial bacterial enzyme, was synthesized and screened against four strains of bacterial pathogens. A phenyl substituent in either  $\alpha$ - or  $\beta$ - position of the tropolone was shown to exhibit the most pronounced inhibitory effect on the enolase activity. To aid in future structure-based drug design efforts, we have determined crystal structure of *E. coli* enolase in the substrate-bound and the mixed apo-substrate-product bound form at 1.8 Å and 2.2 Å respectively. Molecular modeling of selected tropolone derivatives supports the expected electrostatic interactions between the tropolone carbonyl oxygen and the  $Mg^{2+}$  ion.

The central role of enolase in glycolysis, membrane formation and RNA processing suggest that this unexplored target could be a potentially fruitful avenue for development of new, non-cross resistant antibiotics. The tropolone and tropone inhibitors identified in this study showed tunable structure-activity relationships, are synthetically accessible and have a variety of physical properties consistent with good leads for development of agents acting against Gram-negative pathogens. Moreover, they display minimal cytotoxicity towards healthy mammalian cells.<sup>34</sup> There has been significant

success in developing antibiotics with metal binding motifs such as tetracyclines and fluoroquinolones with careful attention paid to potential metabolic liabilities associated with a metal binding moiety and off-target effects. It is important to note that metalloprotein inhibitors are not prone to widespread off-target enzyme inhibition activity but are rather quite selective for their intended targets, including tropolone-based leads. As reported by Fullagar et al., a tropolone derivative designed as an inhibitor of the  $Zn^{2+}$ -dependent metalloenzyme LasB showed high selectivity over other  $Zn^{2+}$ -dependent metalloproteins and simultaneously lost efficacy for Cu-dependent tyrosinase.<sup>22</sup> Also, a rigorous evaluation of the catalytic and structural properties of the metal binding motifs with suitable pharmacokinetics led to development of many HIV integrase inhibitors and other novel antiviral agents.<sup>35,36</sup> As shown in the work by Murelli et al., a careful screening of  $\alpha$ -hydroxytropolones against HIV Reverse Transcriptase Ribonuclease H lead to compounds with good levels of enzymatic inhibition and protective antiviral activity in cell-based assays.<sup>37</sup>

Owing to the rise in antibiotic resistance the need for drugs targeting novel pathways is compelling. Given the potential of this enzyme to serve a new antibiotic target in Gram-negative pathogens, the identification of a lead inhibitor series and the associated structural studies leaves us well-positioned to evaluate inhibition of this pathway. The structure of enolase helps rationalize the structure-activity relationships and will greatly benefit our optimization efforts.

## ACCESSION ID

NCBI: CAA57795.1

UniProtKB: P0A6P9 (ENO\_ECOLI)

## ASSOCIATED CONTENT

The Supporting Information is available free of charge on the ACS Publications website.

## AUTHOR INFORMATION

### Corresponding Author

Dennis Wright

dennis.wright@uconn.edu

## ACKNOWLEDGMENTS

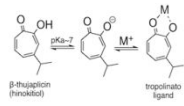
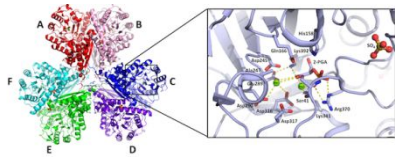
The authors thank the NIH/NIAID for generous support of this work (1R21AI140734-01). Nigel Priestley, Professor of Chemistry, University of Montana for conducting initial evaluation of tropolones antibacterial activity. Amy Florian for providing the confocal microscopy images. This research used resources at the AMX (17-ID-1) beam line of the National Synchrotron Light Source II, a U.S. Department of Energy (DOE) Office of Science User Facility operated for the DOE Office of Science by Brookhaven National Laboratory under Contract No. DE-SC0012704. Use of the Stanford Synchrotron Radiation Lightsource, SLAC National Accelerator Laboratory, is supported by the U.S. Department of Energy, Office of Science, Office of Basic Energy Sciences under Contract No. DE-AC02-76SF00515. The SSRL Structural Molecular Biology Program is supported by the DOE Office of Biological and Environmental Research, and by the National Institutes of Health, National Institute of General Medical Sciences (including P41GM103393). The contents of this publication are solely the responsibility of the authors and do not necessarily represent the official views of NIGMS or NIH.

## REFERENCES

- (1) Ho, J., Tambyah, P. A., and Paterson, D. L. (2010) Multiresistant Gram-negative infections: a global perspective. *Curr. Opin. Infect. Dis.* 23, 546–553.
- (2) Bentley, R. (2008) A fresh look at natural tropolones. *Nat. Prod. Rep.* 25, 118–138.
- (3) O'Shea, R., and Moser, H. E. (2008) Physicochemical properties of antibacterial compounds: implications for drug discovery. *J. Med. Chem.* 51, 2871–2878.
- (4) Morita, Y., Matsumura, E., Okabe, T., Shibata, M., Sugiura, M., Ohe, T., Tsujibo, H., Ishida, N., and Inamori, Y. (2003) Biological activity of tropolone. *Biol. Pharm. Bull.* 26, 1487–1490.
- (5) Morita, Y., Matsumura, E., Tsujibo, H., Yasuda, M., Okabe, T., Sakagami, Y., Kumeda, Y., Ishida, N., and Inamori, Y. (2002) Biological activity of 4-acetyltropolone, the minor component of *Thujopsis dolabrata* Sieb. et Zucc. *Biol. Pharm. Bull.* 25, 981–985.
- (6) Morita, Y., Sakagami, Y., Okabe, T., Ohe, T., Inamori, Y., and Ishida, N. (2007) The mechanism of the bactericidal activity of hinokitiol. *Biocontrol Sci.* 12, 101–110.
- (7) Congreve, M., Carr, R., Murray, C., and Jhoti, H. (2003) A “rule of three” for fragment-based lead discovery? *Drug Discov. Today* 8, 876–877.
- (8) Ononye, S. N., van Heyst, M., Falcone, E. M., Anderson, A. C., and Wright, D. L. (2012) Toward isozyme-selective inhibitors of histone deacetylase as therapeutic agents for the treatment of cancer. *Pharm. Pat. Anal.* 1, 207–221.
- (9) Oblak, E. Z., Bolstad, E. S. D., Ononye, S. N., Priestley, N. D., Hadden, M. K., and Wright, D. L. (2012) The furan route to tropolones: probing the antiproliferative effects of beta-thujaplicin analogs. *Org. Biomol. Chem.* 10, 8597–8604.
- (10) Saleh, N. A., Zwiefak, A., Mordarski, M., and Pulverer, G. (1988) Antibacterial activity of selected tropolones and tropolones. *Zentralbl. Bakteriol. Mikrobiol. Hyg. A.* 270, 160–170.
- (11) Kabsch, W. (2010) XDS. *Acta Crystallogr. D. Biol. Crystallogr.* 66, 125–132.
- (12) Winn, M. D., Ballard, C. C., Cowtan, K. D., Dodson, E. J., Emsley, P., Evans, P. R., Keegan, R. M., Krissinel, E. B., Leslie, A. G. W., McCoy, A., McNicholas, S. J., Murshudov, G. N., Pannu, N. S., Potterton, E. A., Powell, H. R., Read, R. J., Vagin, A., and Wilson, K. S. (2011) Overview of the CCP4 suite and current developments. *Acta Crystallogr. D. Biol. Crystallogr.* 67, 235–242.
- (13) Batty, T. G. G., Kontogiannis, L., Johnson, O., Powell, H. R., and Leslie, A. G. W. (2011) *iMOSFLM*: a new graphical interface for diffraction-image processing with *MOSFLM*. *Acta Crystallogr. Sect. D Biol. Crystallogr.* 67, 271–281.
- (14) Emsley, P., Lohkamp, B., Scott, W. G., and Cowtan, K. (2010) Features and development of *Coot*. *Acta Crystallogr. D. Biol. Crystallogr.* 66, 486–501.
- (15) Murshudov, G. N., Skubak, P., Lebedev, A. A., Pannu, N. S., Steiner, R. A., Nicholls, R. A., Winn, M. D., Long, F., and Vagin, A. A. (2011) REFMAC5 for the refinement of macromolecular crystal structures. *Acta Crystallogr. D. Biol. Crystallogr.* 67, 355–367.
- (16) Schrodinger LLC. (2017) Schrodinger Suite 2017-4 Protein Preparation Wizard. New York, NY.
- (17) Harder, E., Damm, W., Maple, J., Wu, C., Reboul, M., Xiang, J. Y., Wang, L., Lupyan, D., Dahlgren, M. K., Knight, J. L., Kaus, J. W., Cerutti, D. S., Krilov, G., Jorgensen, W. L., Abel, R., and Friesner, R. A. (2016) OPLS3: A Force Field Providing Broad Coverage of Drug-like Small Molecules and Proteins. *J. Chem. Theory Comput.* 12, 281–296.

- (18) Schrödinger, L. (2014) LigPrep. New York, NY.
- (19) Schrödinger, L. (2017) Glide. New York, NY.
- (20) Nakano, K., Chigira, T., Miyafusa, T., Nagatoishi, S., Caaveiro, J. M. M., and Tsumoto, K. (2015) Discovery and characterization of natural tropolones as inhibitors of the antibacterial target CapF from *Staphylococcus aureus*. *Sci. Rep.* 5, 15337.
- (21) Ismaya, W. T., Rozeboom, H. J., Weijn, A., Mes, J. J., Fusetti, F., Wichers, H. J., and Dijkstra, B. W. (2011) Crystal structure of *Agaricus bisporus* mushroom tyrosinase: identity of the tetramer subunits and interaction with tropolone. *Biochemistry* 50, 5477–5486.
- (22) Fullagar, J. L., Garner, A. L., Struss, A. K., Day, J. A., Martin, D. P., Yu, J., Cai, X., Janda, K. D., and Cohen, S. M. (2013) Antagonism of a zinc metalloprotease using a unique metal-chelating scaffold: tropolones as inhibitors of *P. aeruginosa* elastase. *Chem. Commun. (Camb)*. 49, 3197–3199.
- (23) Lomenick, B., Hao, R., Jonai, N., Chin, R. M., Aghajan, M., Warburton, S., Wang, J., Wu, R. P., Gomez, F., Loo, J. A., Wohlschlegel, J. A., Vondriska, T. M., Pelletier, J., Herschman, H. R., Clardy, J., Clarke, C. F., and Huang, J. (2009) Target identification using drug affinity responsive target stability (DARTS). *Proc. Natl. Acad. Sci. U. S. A.* 106, 21984–21989.
- (24) Pai, M. Y., Lomenick, B., Hwang, H., Schiestl, R., McBride, W., Loo, J. A., and Huang, J. (2015) Drug affinity responsive target stability (DARTS) for small-molecule target identification. *Methods Mol. Biol.* 1263, 287–298.
- (25) Bonnin, R. A., and Bouloc, P. (2015) RNA Degradation in *Staphylococcus aureus*: Diversity of Ribonucleases and Their Impact. *Int. J. Genomics* 2015, 395753.
- (26) Kahan, F. M., Kahan, J. S., Cassidy, P. J., and Kropp, H. (1974) The mechanism of action of fosfomycin (phosphonomycin). *Ann. N. Y. Acad. Sci.* 235, 364–386.
- (27) Chandran, V., and Luisi, B. F. (2006) Recognition of enolase in the *Escherichia coli* RNA degradosome. *J. Mol. Biol.* 358, 8–15.
- (28) Taghbalout, A., and Rothfield, L. (2007) RNaseE and the other constituents of the RNA degradosome are components of the bacterial cytoskeleton. *Proc. Natl. Acad. Sci. U. S. A.* 104, 1667–1672.
- (29) Diaz-Ramos, A., Roig-Borrellas, A., Garcia-Melero, A., and Lopez-Aleman, R. (2012) alpha-Enolase, a multifunctional protein: its role on pathophysiological situations. *J. Biomed. Biotechnol.* 2012, 156795.
- (30) Pancholi, V. (2001) Multifunctional alpha-enolase: its role in diseases. *Cell. Mol. Life Sci.* 58, 902–920.
- (31) Leonard, P. G., Satani, N., Maxwell, D., Lin, Y.-H., Hammoudi, N., Peng, Z., Pisaneschi, F., Link, T. M., Lee, G. R. 4th, Sun, D., Prasad, B. A. B., Di Francesco, M. E., Czako, B., Asara, J. M., Wang, Y. A., Bornmann, W., DePinho, R. A., and Muller, F. L. (2016) SF2312 is a natural phosphonate inhibitor of enolase. *Nat. Chem. Biol.* 12, 1053–1058.
- (32) Cho, H., Um, J., Lee, J.-H., Kim, W.-H., Kang, W. S., Kim, S. H., Ha, H.-H., Kim, Y.-C., Ahn, Y.-K., Jung, D.-W., and Williams, D. R. (2017) ENOblock, a unique small molecule inhibitor of the non-glycolytic functions of enolase, alleviates the symptoms of type 2 diabetes. *Sci. Rep.* 7, 44186.
- (33) Jung, D.-W., Kim, W.-H., Park, S.-H., Lee, J., Kim, J., Su, D., Ha, H.-H., Chang, Y.-T., and Williams, D. R. (2013) A unique small molecule inhibitor of enolase clarifies its role in fundamental biological processes. *ACS Chem. Biol.* 8, 1271–1282.
- (34) Ononye, S. N., Vanheyst, M. D., Oblak, E. Z., Zhou, W., Ammar, M., Anderson, A. C., and Wright, D. L. (2013) Tropolones as lead-like natural products: The development of potent and selective histone deacetylase inhibitors. *ACS Med. Chem. Lett.* 4, 757–761.
- (35) Agrawal, A., DeSoto, J., Fullagar, J. L., Maddali, K., Rostami, S., Richman, D. D., Pommier, Y., and Cohen, S. M. (2012) Probing chelation motifs in HIV integrase inhibitors. *Proc. Natl. Acad. Sci.*
- (36) Rogolino, D., Carcelli, M., Sechi, M., and Neamati, N. (2012) Viral enzymes containing magnesium: Metal binding as a successful strategy in drug design. *Coord. Chem. Rev.*
- (37) Murelli, R. P., D'Erasmus, M. P., Hirsch, D. R., Meck, C., Masaoka, T., Wilson, J. A., Zhang, B., Pal, R. K., Gallicchio, E., Beutler, J. A., and Le Grice, S. F. J. (2016) Synthetic  $\alpha$ -hydroxytropolones as inhibitors of HIV reverse transcriptase ribonuclease H activity. *Medchemcomm* 7, 1783–1788.

“For Table of Contents Only”



1  
2  
3  
4  
5  
6  
7  
8  
9  
10  
11  
12  
13  
14  
15  
16  
17  
18  
19  
20  
21  
22  
23  
24  
25  
26  
27  
28  
29  
30  
31  
32  
33  
34  
35  
36  
37  
38  
39  
40  
41  
42  
43  
44  
45  
46  
47  
48  
49  
50  
51  
52  
53  
54  
55  
56  
57  
58  
59  
60